POTSDAM-INSTITUT FÜR KLIMAFOLGENFORSCHUNG

Network percolation provides early warnings of abrupt changes in coupled oscillatory systems: An explanatory analysis

Noémie Ehstand [1,*] Reik V. Donner [2,3] Cristóbal López [1] and Emilio Hernández-García [1]

[1]*IFISC (CSIC-UIB), Instituto de Física Interdisciplinar y Sistemas Complejos, Campus Universitat de les Illes Balears, E-07122 Palma de Mallorca, Spain*

[2]*Department of Water, Environment, Construction and Safety, Magdeburg-Stendal University of Applied Sciences, Breitscheidstraße 2, D-39114 Magdeburg, Germany*

[3]*Research Department IV–Complexity Science and Research Department I–Earth System Analysis, Potsdam Institute for Climate Impact Research (PIK)–Member of the Leibniz Association, Telegrafenberg A31, D-14473 Potsdam, Germany*

(Received 10 May 2023; accepted 2 October 2023; published 7 November 2023)

Functional networks are powerful tools to study statistical interdependency structures in spatially extended or multivariable systems. They have been used to get insights into the dynamics of complex systems in various areas of science. In particular, percolation properties of correlation networks have been employed to identify early warning signals of critical transitions. In this work, we further investigate the corresponding potential of percolation measures for the anticipation of different types of sudden shifts in the state of coupled irregularly oscillating systems. As a paradigmatic model system, we study the dynamics of a ring of diffusively coupled noisy FitzHugh-Nagumo oscillators and show that, when the oscillators are nearly completely synchronized, the percolation-based precursors successfully provide very early warnings of the rapid switches between the two states of the system. We clarify the mechanisms behind the percolation transition by separating global trends given by the mean-field behavior from the synchronization of individual stochastic fluctuations. We then apply the same methodology to real-world data of sea surface temperature anomalies during different phases of the El Niño-Southern Oscillation. This leads to a better understanding of the factors that make percolation precursors effective as early warning indicators of incipient El Niño and La Niña events.

DOI: 10.1103/PhysRevE.108.054207

I. INTRODUCTION

The occurrence of sudden shifts between radically different dynamical regimes is a striking phenomenon displayed by a variety of complex systems, including climatic [1–4], ecological [5,6], financial [7,8], and physiological [9] ones. These so-called critical transitions or regime shifts can have large impacts, as they bring about a drastic change in the function and structure of the systems undergoing them. Their forecast well in advance is of utmost importance for risk management and the mitigation of their impacts.

A large body of research has been devoted to the identification of generic early warning signals for upcoming critical transitions [10–16] and their conceptualization is well developed for transitions induced by bifurcations, accordingly named B-tipping in the nomenclature of Ashwin *et al.* [4]. In such a situation, a control parameter is changed gradually, until eventually a critical threshold or tipping point is reached at which the system suddenly reorganizes into a completely new dynamical regime. Dynamical systems theory shows that this occurs as the state of the system looses stability, which forces it to move to a new attractor. In most cases [3], as the system approaches the point of loss of stability, the dominant eigenvalue of its Jacobian matrix tends to zero, which translates into decreasing relaxation rates towards equilibrium when the system is perturbed [17–19]. This phenomenon is known as critical slowing down [20].

A variety of early warning indicators for critical transitions have been proposed based on statistical signatures of critical slowing down, including temporal [21–28] and spatial indicators [29–31]. In addition, some studies have integrated both spatial and temporal indicators [32]. Alongside these developments, many studies have demonstrated the potential of complex networks for the study of statistical structures in systems consisting of interconnected units [33–37]. In particular, various works have used network-based frameworks for the prediction of bifurcation-induced tipping [38–40]. In Rodriguez-Mendez *et al.* [40] functional networks representing strong correlations between different sites in spatially extended systems were studied and different percolation quantifiers in such networks were shown to provide useful anticipation of an incipient bifurcation.

More specifically, in systems consisting of interconnected (e.g., spatially distributed) units coupled by diffusive or similar types of homogenizing interactions, as a bifurcation is approached, the variability between different units becomes increasingly correlated as a consequence of the slowdown mentioned above (there is an increasing amount of time for the coupling to act). Such an increased coherence can manifest in the dynamics at different timescales, from a synchronization of fast fluctuations up to the emergence of common long-term

*n.ehstand@ifisc.uib-csic.es

behaviors (e.g., stochastic trends). In a correlation-based functional network this translates into an increase of the link density. Hence, as conditions bring the system closer to the bifurcation, the increasing connectivity eventually results in the development of a large connected component comprising a significant fraction of all nodes. This is called percolation. Full connectivity of the network is attained at the bifurcation but the percolation threshold is actually reached *before* the bifurcation. In this way, percolation of the functional network is an early warning signal of the approaching bifurcation, and precursor signals of the percolation transition itself will provide even earlier anticipation than standard anticipatory signals of the bifurcation. The success of this approach was well illustrated, for various B-tipping situations, in Rodriguez-Mendez *et al.* [40].

Despite their generic nature and relevance across disciplines, not all interesting or important sudden transitions in complex systems are of the B-tipping type [4,41]. For instance, the regime shift may be induced by noisy fluctuations, not necessarily close to any bifurcation point, making the system jump to an alternative dynamic attractor. This is known as N-tipping. In other cases, the attractor changes as the governing parameter is varied. If the rate of change of the parameter is too fast, then the system may leave the basin of attraction, leading to so-called R-tipping. Further, Kuehn [42] considered tipping-like situations induced by the bifurcation of the fast dynamics in two timescale systems. Whether generic early warning signs of sudden shifts can be found beyond the case of B-tipping remains an open question and represents a significant challenge.

In this paper, we explore the ability of percolation measures based on functional network representations to anticipate sudden shifts in spatially extended complex systems beyond the classical B-tipping scenario, focusing specifically on systems presenting irregular oscillations. We first consider fast-slow systems, choosing as a leading example a system consisting of nonperiodic, stochastic FitzHugh-Nagumo oscillators coupled by diffusion and arranged in a one-dimensional ring lattice. All model parameters remain fixed so that no bifurcation or B-tipping occurs. Nevertheless, jumps between distinct global states occur at irregular times, for which we want to find anticipatory signals. To this end, we construct a time-dependent functional network describing the evolution of correlations of the system's fast variables at different locations. We show that percolation transitions occur in the network, which anticipate the irregular sudden changes between different stages of the system's oscillation. We then characterize the contributions of different processes potentially causing the percolation transitions. These include common trends among individual oscillators as well as the synchronization of the superimposed (stochastic) fluctuations.

The obtained results provide new insights into time-dependent structural changes emerging in functional network representations of multicomponent complex systems which lead to a better understanding and interpretation of the percolation-based precursors in their application to real-world oscillatory phenomena. This is illustrated by reconciling the previously reported anticipatory power of the percolation framework in the climatic phenomena of El Niño and La Niña. Notably, Rodriguez-Mendez *et al.* [40] applied the percolation-based framework to time series of sea-surface temperatures (SSTs) in the equatorial Pacific. They showed the ability of the methodology to anticipate El Niño and La Niña events, the two extreme stages of a single climate oscillation: the El Niño-Southern Oscillation (ENSO). Other works have also confirmed that different characteristics of the percolation transition on climate networks provide early warning indicators for the occurrence of El Niño or La Niña [43–46]. In fact, several topological as well as geometric properties of functional climate networks have been reported to provide useful diagnostics for the overall state of the spatially extended coupled atmosphere-ocean system during different ENSO phases [47–49]. Nonetheless, the mathematical mechanisms leading to the percolation transition in these correlation networks are far from being fully understood. In light of the understanding gained from studying the processes causing the percolation transitions in the FitzHugh-Nagumo system, we identify the mechanism behind the performance of the percolation framework for the anticipation of El Niño and La Niña reported in Rodriguez-Mendez *et al.* [40]: a global tendency in the variation of SSTs across the considered region.

The remainder of this paper is organized as follows. In Sec. II we describe the network construction and the principles of percolation-based precursors for critical transitions. Section III first introduces the system of coupled FitzHugh-Nagumo oscillators and describes its numerical integration. The application of the percolation-framework to this system and the results obtained are then detailed. Finally, in Sec. IV, we show how the lessons learned from the previous example shed light on the dynamical processes inducing variations in the connectivity structure of the (correlation-based) functional network describing El Niño and other phases of the El Niño-Southern Oscillation.

II. CORRELATION NETWORKS AND PERCOLATION

A. Functional networks

Spatially extended dynamical systems can be approximated by spatially localized units governed by their own local dynamics while interacting with other units through processes such as diffusion, convection, conduction, etc. Functional networks are a discrete way of encoding statistical associations among these individual local dynamics. They have been successfully employed to get insights into the dynamics of complex systems in fields as diverse as neurophysiology [50], urban systems [51], seismology [52], and climatology [35,37,53].

In this paper, we analyze the emergence of strong correlations between different locations of spatially extended dynamical systems by means of a functional network constructed as follows. Let the spatiotemporal field $u(x,t)$ describe (although perhaps only in an incomplete manner) the evolution of the system's state, where x is space and t is time. We discretize both space and time to obtain the series $\{u_k(t_l)\}_{kl}$, where $k \in \{1,\ldots,N\}$ labels the different spatial locations that will be used as the N nodes of the functional network, and $l \in \{1,\ldots,R\}$ labels time instants. The links are built through statistical analysis of inter-dependencies between pairs of time series from different spatial locations.

Most commonly, the similarity between the variability at locations a and b is computed via the zero-lag Pearson correlation

$$\rho_{ab} = \frac{\sum_l p_a(t_l) p_b(t_l)}{\sqrt{(\sum_l p_a(t_l)^2)(\sum_l p_b(t_l)^2)}}, \tag{1}$$

where $p_k(t_l) = u_k(t_l) - \frac{1}{R}\sum_l u_k(t_l)$ is the deviation of the field from its temporal mean at each location. A link is set between the nodes a and b if the Pearson correlation is higher than a given threshold γ: $\rho_{ab} > \gamma$. Only positive correlations are considered here, but it is straightforward to extend the formalism to the case $|\rho_{ab}| > \gamma$, as was done in Ekhtiari *et al.* [54] for instance.

The (undirected) network constructed in this manner describes the strongest positive linear correlations between parts of the system over the time interval $[t_1, t_R]$. We call this the "network at time t_R," stressing that it contains information only on the past of time t_R, as adequate for a formalism that will be intended for forecasting and anticipation. By repeating the procedure over consecutive intervals $[t_2, t_{R+1}]$, $[t_3, t_{R+2}]$, etc., we construct networks at times t_{R+1}, t_{R+2}, etc., a sequence that conforms a time-dependent functional network [47], a particular type of a temporal network [55] whose architecture reflects the evolution of the correlations of the system evaluated over time windows consisting of R time steps each. Hence, by analyzing how the network's topological properties change over time, it is possible to detect a reorganization of the correlation structure of the system at a certain time, revealing changes in the spatiotemporal dynamics.

We note that the above network construction method is just the simplest among the many available methodologies that use network-theory frameworks to reveal dynamical properties of spatially extended dynamical systems (see, e.g., Ref. [35]). Other measures of statistical dependence, such as lagged correlations [43,46], or information-theoretic measures [56] can be used, which may lead to functional networks encoding different aspects of time series similarity [57]. But here we restrict ourselves to the simplest methodology, which can be applied with essentially no knowledge on the underlying mechanisms or on the spatial and temporal scales generating the spatiotemporal signals. We will show that this framework is powerful enough to find anticipatory signals of sharp transitions, as well as to extract some information on their origin.

B. Percolation

Percolation theory traditionally describes the changes in network connectivity as links are added or removed [34,58]. In many networks, provided that they are large enough, there is a critical number of links at which the disconnected clusters merge into a larger connected cluster that contains a significant fraction of the nodes. Such phenomenon is referred to as a percolation transition. Several metrics can be used to characterize the cluster properties of a network [34]. In particular, we consider here the *relative size of the largest connected component*, S_1, i.e., the fraction of nodes that forms the largest cluster, and the *probability that a randomly chosen node belongs to a cluster of size s*, c_s, $s \neq 1$. The later quantity can be expressed as

$$c_s = \frac{s n_s}{N}, \tag{2}$$

where n_s is the number of clusters of size s and N is the number of nodes in the network. Monitoring such characteristics in the time sequence of evolving functional networks allows to identify and potentially anticipate percolation transitions in time-dependent networks.

Percolation measures from correlation networks have been shown to provide very early warning signals of upcoming B-tipping in spatially extended systems [40]. Notably, critical slowing down occurs close to various (although not all [3]) types of bifurcations. As already mentioned in the introduction, in systems consisting of interconnected spatial units with homogenizing interactions (such as diffusive coupling), the slowing down of the dynamics when approaching a bifurcation gives ample time for the interactions to produce large correlations, which in turn lead to a correlation network with large link density. Eventually, the increasing connectivity will result in a percolation transition in the functional network. The percolation threshold is reached *before* (i.e., at lower connectivity than) the bifurcation (at which full connectivity is attained). Thus, the occurrence of a percolation transition as a system parameter is changed is already an early warning signal announcing the proximity of a bifurcation; and anticipatory signals of the percolation itself will provide still earlier warning signals of the approaching bifurcation or B-tipping. Rodriguez-Mendez *et al.* [40] illustrate this approach for various B-tipping situations.

However, many important sudden shifts in nature cannot be attributed to B-tipping processes. In the following, we therefore investigate the potential of the percolation measures for anticipating sudden shifts in spatially extended complex systems beyond the case of B-tipping, focusing specifically on systems presenting irregular oscillations. The aim will be to anticipate associated abrupt changes in the system state that occur during the oscillation cycles.

III. DIFFUSIVELY COUPLED NOISY FITZHUGH-NAGUMO OSCILLATORS

A. Description of the model

The FitzHugh-Nagumo (FN) system is a minimalistic and prototypical model of an excitable system which can display an oscillatory regime. It is a simplification of the Hodgkin-Huxley model for the transmission of electrical pulses along a nerve axon [59] which was first derived by FitzHugh [60] and Nagumo [61]. The archetypal form of the model is given by

$$\begin{aligned} \dot{u} &= f(u) - v + I, \\ \tfrac{1}{\epsilon}\dot{v} &= u - bv + c, \end{aligned} \tag{3}$$

where $f(u) = \alpha u(u-a)(1-u)$ and α, a, b, c, I are constant parameters. The excitable variable u, corresponding in the original model to the membrane's potential, is characterized by a fast dynamics while the recovery variable v has a slow dynamics. The timescale separation between both variables is given by $\epsilon \ll 1$. Depending on the choice of parameters, system (3) has one or three stationary points, whose stability determines the solution's behavior. For the set of parameters

chosen in this study (which includes $I = c = 0$), the system exhibits an unstable focus located at (0,0) as well as a unique attractive limit cycle, leading to periodic pulses. This type of oscillations are of primary importance for the modeling of neuro-biological systems [50,60,61], in electrical circuits [62], in seismology [63], and in climate science [64].

In this study, we consider a system consisting of N nonperiodic and stochastic FN-type oscillators coupled by diffusion on a one-dimensional ring lattice. The time evolution of the state (u_k, v_k) at node k is described by

$$\begin{aligned} \dot{u_k} &= f(u_k) - v_k + I + (\Delta u)_k + \sqrt{2D^{(u)}}\eta_k^{(u)}, \\ \tfrac{1}{\epsilon}\dot{v_k} &= u_k - bv_k + c + (\Delta v)_k + \sqrt{2D^{(v)}}\eta_k^{(v)}, \end{aligned} \tag{4}$$

for $k = 1, ..., N$. We will refer to the label k as "space" in the following. Node k is coupled to its nearest neighbor on each side via the diffusive terms $(\Delta u)_k = u_{k+1} + u_{k-1} - 2u_k$ and $(\Delta v)_k = v_{k+1} + v_{k-1} - 2v_k$. To avoid unnecessarily complex dynamics we have chosen the diffusion coefficients of the u and v variables to be equal, and units of space are scaled so that this common diffusion coefficient becomes unity. The terms $\eta_k^{(u)}(t)$ and $\eta_k^{(v)}(t)$ are two independent Gaussian white noise sources, with $\langle \eta_r^{(a)}(t)\eta_s^{(b)}(t')\rangle = \delta_{ab}\delta_{rs}\delta(t - t')$. The addition of noise to the deterministic system is motivated by the fact that real systems unavoidably include stochastic fluctuations and by the necessity of well-defined spatial correlation functions for the construction of the correlation network described in Sec. II. Despite the presence of these additive noise terms, if their intensity remains small, the resulting FN dynamics is a rather regular periodic oscillation. To bring the model closer to the type of irregular oscillations that we want to address—for which prediction is a nontrivial task—we let the parameter ϵ, which has the most direct influence on the timescale separation between u and v, vary stepwise in time. Precisely, ϵ takes a constant value during the time needed for the system to complete a full oscillation cycle. In this case, a full oscillation cycle is defined as a full cycle of the mean dynamics over all N oscillators. Once a cycle has been completed, a new value of ϵ is chosen (the same for all k) with uniform probability over the interval (0.001, 0.033). The range is chosen such as to produce oscillations with period lengths suited to the purpose of our study. This choice of $\epsilon = \epsilon(t)$ introduces a strong irregularity in the period of the oscillations making the system more similar to natural oscillatory phenomena, and making the anticipation of the different abrupt changes substantially more challenging.

B. Numerical integration

In the following, we choose $\alpha = 1, a = -1, b = -0.83$, $c = 0, I = 0$ and noise intensities $D^{(u)} = D^{(v)} = 0.01$. We consider $N = 500$ oscillators.

To compute numerically the solution to System (4), we start from a uniform initial state $(u_k(0) = -0.16, v_k(0) = 0.01)\ \forall\ k \in \{1, \ldots, N\}$. The solution is evolved with an integration time step $dt = 0.05$. At each time step the deterministic part of the equation is integrated first via a fourth order Runge-Kutta scheme [65, Sec. 7.4]. Then, N independent random Gaussian distributed numbers of zero mean and variance $2D^{(u)}dt$ and $2\epsilon^2 D^{(v)}dt$ are added to u_k and v_k, $k \in \{1, \ldots, N\}$, respectively.

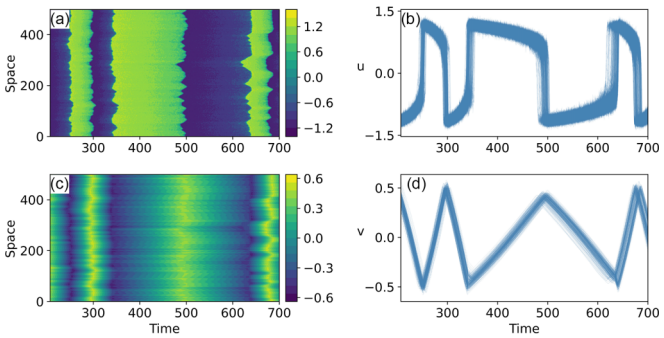

FIG. 1. Left: evolution of the fields u (a) and v (c) as a function of space and time. Right: all ($N = 500$) individual time series superimposed for u (b) and v (d).

Figure 1 shows the evolution of the solution (u, v). Figures 1(a) and 1(c) show the evolution of the fields u and v as a function of space and time. As an alternative view, Figs. 1(b) and 1(d) show the individual time series of u and v superimposed for all ($N = 500$) nodes. The evolution of the variables u and v is quite coherent in space, i.e., all nodes k are nearly perfectly synchronized, a consequence of the diffusive coupling and of the choice of parameters. We observe that the state variable u presents asymmetric and nonperiodic oscillations with sudden switches between positive/negative values. The state variable v shows linear increase and decrease in time.

In the next section, we investigate the potential of the percolation precursors to anticipate the irregular abrupt global changes in the state of the fast variable u, without using any information on the variable v. To do so, we construct a sequence of networks from the discrete field $u_k(t_l)$ following the methodology described in the previous section, using consecutive time windows of 140 steps, that is of seven time units $(140 \times dt)$, and a correlation threshold $\gamma = 0.6$. Information from the field $v_k(t_l)$ is ignored in the network construction. As mentioned previously, the network (and network quantities) at time t describes the information contained in the time window prior to t.

Note that the predictability of the behavior of u is made significantly more challenging by (1) the time dependence of ϵ which leads to the irregularity of the oscillations, as well as (2) the absence of information from the field v in the network construction.

C. Percolation-based precursors in the FN system

The increase in spatial variance is commonly used as a precursor of abrupt changes in dynamical systems [29,30]. Therefore, we first compute the variance of the state variable u as $\bar{\sigma}_u(t_l) = \sqrt{\frac{1}{N}\sum_{k=1}^{N}[u_k(t_l) - \bar{u}(t_l)]^2}$, where $\bar{u}(t_l) = \frac{1}{N}\sum_{k=1}^{N} u_k(t_l)$ is a spatial average (over all the nodes). Figure 2(a) shows again the evolution of the u_k time series at all nodes for reference. The gray shading in Figs. 2(b), 2(c), and 2(d) indicates the time intervals during which the values of u are changing sign, the bounds of this interval being defined by

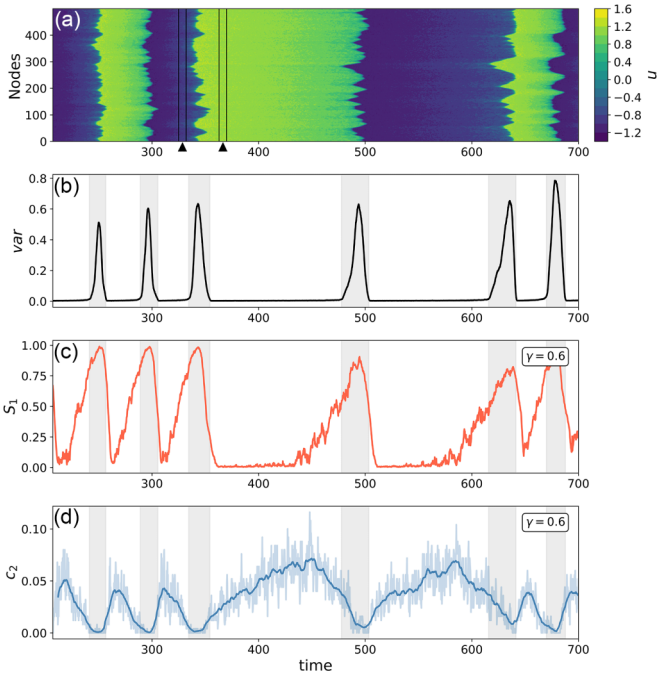

FIG. 2. (a) Spatiotemporal evolution of the variable u, (b) spatial variance of u, (c) relative size S_1 of the largest connected component in the network constructed from the variables u_k with correlation threshold $\gamma = 0.6$, (d) probability c_2 that a randomly chosen node belongs to a component of size 2 in the network. The light blue line gives the raw values of c_2 whereas the darker curve smooths the data using a 40-point window average (i.e., 2 time units), centered at the time of interest. The gray shading indicates the time interval during which the u_ks switch sign. The two triangles indicate the locations of two time intervals of 140 time steps each whose correlation properties are displayed in Fig. 4.

the first and the last oscillator to cross zero. In Fig. 2(b) we can see that the variance peaks within this interval. However, there is no detectable rise of spatial variance until the system enters the "jump" time interval, i.e., until the first oscillators switches sign. Hence, for this system, the peak in variance indicates the occurrence of the abrupt change, but it is not useful as an anticipatory or early warning tool.

Figures 2(c) and 2(d) show the evolution of the network measures S_1, the relative size of the largest connected component, and c_2, the probability that a randomly chosen node belongs to a component of size 2 [40]. Note that in Fig. 2(d) the light blue curve shows the actual values of c_2 while the dark blue curve gives a smoothing of the data which makes the general increase and decrease in the values of c_2 more apparent. The smoothing is obtained using a 40-point window average (the equivalent to two time units), centered at the point of interest.

We observe that both S_1 and c_2 anticipate the abrupt increases and decreases in the state variable associated with the system's oscillations. Precisely, S_1 starts increasing (indicating the start of the percolation phase) long before the sharp changes in the values of u_k. It reaches its maximum during the transition of the state variable and then decreases very rapidly, reaching 0 just after the transition. The behavior of S_1 reflects that the correlation between the dynamics at individual nodes increases as a jump in the u values is approached and accordingly the link density in the network also increases so that eventually a cluster of significant size forms. The numbers of nodes in clusters of small sizes (2, 3, 4, etc.) first increase, before decreasing again as most of the nodes begin to attach to the percolating cluster of relative size S_1. This leads to the presence of a peak in the values of c_2 just as S_1 starts increasing [Fig. 2(d)], providing a very early warning signal of the abrupt change in u. Note that the asymmetry of S_1 around the jump and the lack of peaks in c_2 after the shift are due to the irreversibility of the system's abrupt jumps: the correlation state in the network changes completely after u_k has switched sign for all oscillators.

Despite the irregularity of oscillations and the fact that information from the variable v was ignored in the network construction, the network measures are well able to anticipate the abrupt changes in the values of u. However, we saw that the spatial variance did not provide significant anticipation. This shows the advantage of using the percolation measures as precursors of abrupt changes in the present system.

D. Processes leading to percolation

The occurrence of percolation in the system's functional network, manifested in the increase in S_1 before the abrupt global jump in the oscillator's state occurs, reflects an increase in correlations which can be triggered by two different processes (or by a combination of the two):

(i) From the definition of the spatial Pearson coefficient in Eq. (1) it is clear that a large and coherent change common to all spatial units gives a much larger value of ρ_{ab} than small fluctuations around some stationary base state. Thus, in systems for which an abrupt change in the global state of the system is preceded by an upward/downward trend of all spatial units, percolation in the correlation network will occur giving an early warning of the incipient sudden jump. This is a rather general mechanism, that should provide anticipatory signals in a variety of real systems in which sharp global changes interrupt relatively quiescent states.

(ii) In the particular case of the FN system, an additional mechanism could be at work. As already mentioned, u and v evolve on two different timescales. From the structure of the local equation (3), the "slow" variable v can be seen as a bifurcation parameter that drives the dynamics of the "fast" variable u [66]: u drifts slowly until v crosses a critical threshold, which produces an effect similar to a saddle-node bifurcation of the u dynamics. As a consequence, a rapid shift occurs to an alternative u state. In fact, one can clearly anticipate the jumps in u, even if irregular, by looking at the trend in v and estimating when it will reach a critical value (see Fig. 1). This is why we have ignored the information about v in the network construction, to be closer to real-world situations in which relevant variables may not be directly observable. The situation here is very similar to the B-tipping described earlier. The critical slowing down associated to the effective bifurcation in u can thus explain the increase in correlations and the percolation anticipating every sudden jump. This second mechanism is solid and theoretically well understood, but is not as general as the first one, as it will only

be present in fast-slow dynamical systems (which are indeed commonly used to model critical transitions [42]).

We aim to elucidate which of the two mechanisms above (or which combination of them) is responsible for the success of the percolation framework in anticipating the FN system transitions. To this end, we propose to repeat the percolation analysis with modified spatiotemporal data in which all the synchronous upward/downward trends have been removed, and thus any remaining anticipatory power should arise from mechanism (ii) alone. More specifically, we remove the upward/downward trends from the time series at each location k in our coupled FN model by using a Gaussian kernel. That is, for each time step t_l of the time series at k, $u_k(t_l)$, we remove the weighted average:

$$\frac{1}{\sum_{l'} \omega_{l'}^{(l)}} \sum_{l'} \omega_{l'}^{(l)} u_k(t_{l'}), \tag{5}$$

where $\omega_{l'}^{(l)} = \exp[-(t_l - t_{l'})^2/(2b^2)]$ and the bandwidth is b=40 (corresponding to 2 time units). The time window is centered around t_l to remove trends in the best possible way. This implies taking into account some future values to obtain the detrended time series at t_l. This is not a problem since in this subsection we are only interested in elucidating the mechanism for the success of the percolation early warnings, and for this we are postprocessing the whole time series. The finding of the anticipatory signals themselves was properly done in Sec. III C by using only past values of the analyzed time series, as appropriate for real-time monitoring applications.

The residual variability is shown in Fig. 3(a). The time-series of S_1 and c_2 for the network constructed on the detrended fluctuations are shown in Figs. 3(b) and 3(c). The gray shadings bound the jump regions where transient effects remain due to large variations in the data which impede complete detrending. Because of the detrending, mechanism (i) should be absent, and only mechanism (ii) should be at work, at least outside the gray shaded regions. We observe that the anticipation power is similar to the one obtained using the original (i.e., nondetrended) data. This result suggests that critical slowing down indeed takes place in this system before every sudden shift, leading to increased spatial correlations. Note, however, that the chosen correlation threshold is now of $\gamma = 0.536$ versus $\gamma = 0.6$ in the above example. In fact, the strength of the correlations between spatial points should be generally lower when the network is constructed from detrended data, that is when mechanism (i) is absent.

Figure 4 further illustrates the effect of mechanism (i) on the correlation values by inspecting their distributions over two different time intervals during the evolution of the system, characterized, respectively, by high [Figs. 4(a)–4(d)] and low [Figs. 4(e)–4(h)] common trends among the individual dynamics. First, Figs. 4(a)–4(d) characterize the system's correlations over the time interval [325,332] (see first marker in Figs. 2 and 3), that is just before a jump in the values of u. The correlation matrices for the original and detrended data are plotted in Figs. 4(a) and 4(c), respectively. The higher correlation values and more complex structure of the nondetrended case [Fig. 4(a)] are evident. To get a more objective comparison of the correlation values, we show the probability density of values in Fig. 4(b) for both cases as well as their cumulative distributions in Fig. 4(d). These confirm the previous observation: the correlations computed from the original data are overall much higher than the ones computed from the detrended data. Thus, in addition to the fluctuation synchronization observed in the detrended data [mechanism (ii)], there is also a large global trend common to the dynamics of all spatial units in the nondetrended case [mechanism (i)] when the system is close to a transition.

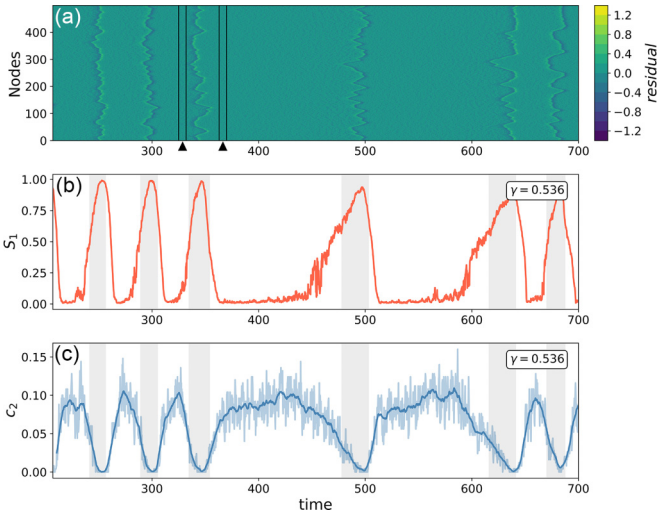

FIG. 3. (a) Residual fluctuations obtained after detrending the variables u_k, (b) relative size S_1 of the largest connected component in the network constructed from the detrended time series for u_k with correlation threshold $\gamma = 0.536$, (c) probability c_2 that a randomly chosen node belongs to a component of size 2. The light blue line gives the raw values of c_2 whereas the darker curve smooths the data using a 40-point window average (i.e., two time units), centered at the time of interest. The gray shading indicates the time interval during which the u_ks switch sign. The two triangles indicate the locations of two time intervals of 140 time steps each whose correlation properties are displayed in Fig. 4.

This interpretation is further confirmed by Figs. 4(e)–4(h), which display the same quantities as Figs. 4(a)–4(d) but over the the time interval [363–370]. This is just after the jump and relatively far from the next one (see second marker in Figs. 2 and 3). In this interval, the upward/downward trend of all spatial units is not as marked and little differences are observed in the structures and distributions of correlations between the original and detrended case.

Note that the difference in correlation strengths between the original data and detrended data illustrated in Figs. 4(a)–4(d) clearly affects the link density in the network. In fact, for any choice of the correlation threshold γ, a larger fraction of correlation values ρ_{ab} will satisfy the criterium $\rho_{ab} > \gamma$ when these correlations are computed from the original data than from the detrended data. This leads to higher network connectivity in the former case and the choice of different thresholds γ in Figs. 2 and 3.

The results presented in this section demonstrate that the rise of the percolation measures in the network computed from the original data (reflecting a rise of correlation in the FN system) is supported by both processes (i) and (ii), although

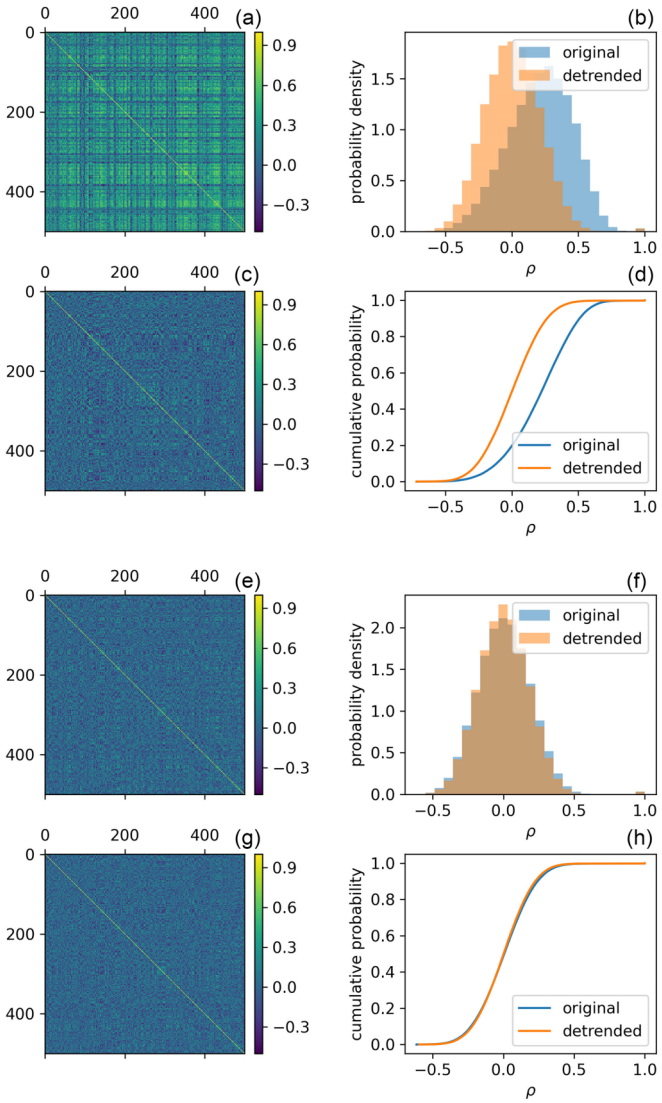

FIG. 4. (a–d) Correlations computed from the original and detrended data over the time interval [325,332] indicated by the first black triangle in Figs. 2 and 3. Panels (a) and (c): the correlation matrices computed from the original and detrended data respectively. Panels (b) and (d): comparison of the correlation distributions (probability density and cumulative probability) for the two cases. Panels e-h: correlations over the time interval [363–370] indicated by the second black triangle in Figs. 2 and 3. Panels (e) and (g): correlation matrices computed from the original and detrended data. Panels (f) and (h): comparison of the correlation distribution and the cumulative distributions.

the presence of mechanism (ii) is powerful enough on its own to provide clear anticipatory signals [Fig. (3)].

Distinguishing the contribution from each process allows us to better understand the behavior of the percolation precursors and the situations in which they are useful beyond the case of the FN system. Specifically, the percolation measures have the potential to detect a global trend in the dynamics of any extended system very early on. Thus, given the knowledge that an increasing/decreasing global trend precedes an abrupt change in the state of the system, the sensitivity of the percolation measures can be leveraged to design very early warnings of upcoming shifts. Moreover, in systems in which some slowing down of the dynamics occurs before the jumps, the anticipatory signals become still more powerful. A postprocessing of the spatiotemporal series helps to reveal the main mechanism of the percolation transition, thus informing about system dynamics. This later point is illustrated further in the next section using a real-world climate example.

IV. PERCOLATION IN SEA SURFACE TEMPERATURE NETWORKS DURING EL NIÑO AND LA NIÑA EVENTS

El Niño and La Niña are the hot and cold phases of ENSO, the dominant interannual oscillation in the tropical Pacific, which affects the whole Earth climatic system [67]. The average ENSO period is about 4 years, but with strong variability which makes its prediction challenging [68,69].

Several studies, using different data sets, variables, network construction methods, and percolation indicators [40,43–46] demonstrate that a percolation transition often occurs in climatic variables of the tropical Pacific before El Niño and La Niña events. However, there is no obvious parameter change during the ENSO cycle that could explain the performance of these indicators as arising from the crossing of a bifurcation or B-tipping. In fact, while a Hopf bifurcation is present in some models of ENSO [67], such that its dynamics can be conceptualized either as subcritical oscillations excited by noise, or supercritical noisy oscillations, the sharp changes that define the El Niño and La Niña events themselves cannot readily be identified as the crossing of any bifurcation.

In the previous section, we showed that, when the system of coupled FN oscillators approaches an abrupt change, the spatial correlations increase and that two combined factors could lead to this increase, namely the effect of a common trend in the monitored variables, or the impact of slowing down of the dynamics when approaching the event. In light of these observations, we now investigate the following question: "Is the 'ENSO-percolation' related to a global trend in the tropical climatic variables or due to critical slowing down on particular phases of the dynamics?"

To answer this question, we build on the network studies of [40] and compare the evolution of the percolation measures for a network computed from sea surface temperatures (SSTs) over the tropical Pacific and from the detrended SSTs over the same region. Precisely, the SST data is obtained from the European Center for Medium-Range Weather Forecast (ECMWF), ERA-Interim reanalysis product [70], a global data set, covering a period of 40 years: from January 1979 to August 2019. We choose 3618 network nodes lying on a $0.375^\circ \times 0.375^\circ$ grid in the region 5S-5N/120W-170W—that is the region of the Pacific used in the computation of the commonly employed NINO3.4 index. The domain is illustrated in Fig. 5. At each node, daily SST anomalies are computed by subtracting the mean seasonal cycle. The links of the network are set based on the correlation of the anomaly time series over a sliding window of 200 days resulting in a time-dependent network.

We focus on three periods: July 1987–July 1988, October 1996–April 1998, and September 2009–January 2011. The mean SST anomalies over the considered region are

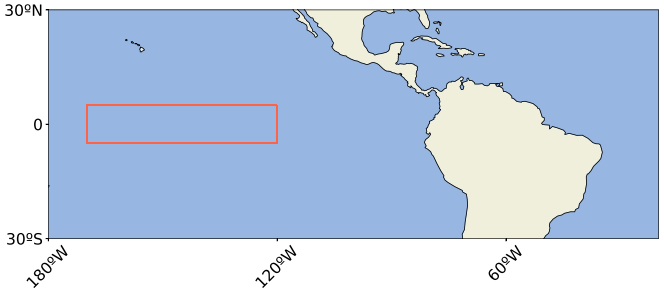

FIG. 5. The red box indicates the region (5S-5N/120W-170W) over which the mean sea surface temperature is monitored in the NINO3.4. index. The nodes of the functional network are chosen on a regular $0.375^\circ \times 0.375^\circ$ grid in this region (see text).

indicated by the gray curves in Fig. 6. The abrupt drops and increases in temperature correspond to La Niña and El Niño events, respectively. These events are commonly defined by five consecutive 3-month running mean values of sea surface temperature (SST) anomalies in the Niño 3.4 region below (above) the threshold of -0.5°C ($+0.5^\circ$C). The starting date, i.e., the first day of the first month, of each event is indicated by a vertical dashed line in the figure.

The relative size of the largest connected component of the network computed from the SST anomalies is shown in Figs. 6(a)–6(c) (red curves) for correlation threshold $\gamma = 0.999$ for the 1988, 1997, and 1998 events and $\gamma = 0.998$ for the 2010 event. The high correlation thresholds are necessary here to prevent the network from being fully connected and hence to observe changes in the network measures S_1 and c_2. We clearly see the increase in S_1 right before every event as reported in Ref. [40]. In addition, Figs. 6(d)–6(f) (blue curves) show the probability for a randomly chosen node to belong to a component of size 2, c_2. This quantity provides additional anticipation indicated by the gray shading in the figure. Precisely, the anticipation provided by c_2 is of 146 days for the event in 1988, 79 days for the event in 1997, 214 days for the event 1998, and 119 days for the event in 2010.

Next, we want to identify which is the mechanism—global trend or fluctuation synchronization by critical slowing down—which leads to the observed percolation transition. To this end, as in the case of the FN oscillators, we postprocess the spatiotemporal series to detrend them at each grid point using a Gaussian kernel with a bandwidth of 60 days. The detrending is illustrated in Figs. 7(a)–7(c) by showing, in gray, the spatial mean of the fluctuations for each considered period. Figures 7(a)–7(c) also show the time series of S_1 (in red) for the network computed from the detrended data for the same correlation thresholds as above. We observe the lack of peak in S_1 [except perhaps in Fig. 7(b)]. To make sure that the absence of signal in S_1 is not due to the choice of γ, we show the values of S_1 for a range of thresholds in Figs. 7(d)–7(f). In all cases the lack of clear structures in the measure confirms the lack of variation in the correlation of the fluctuations preceding ENSO episodes. We note however that a drop in correlations occurs after the La Niña event in the 2009–2011 period, which

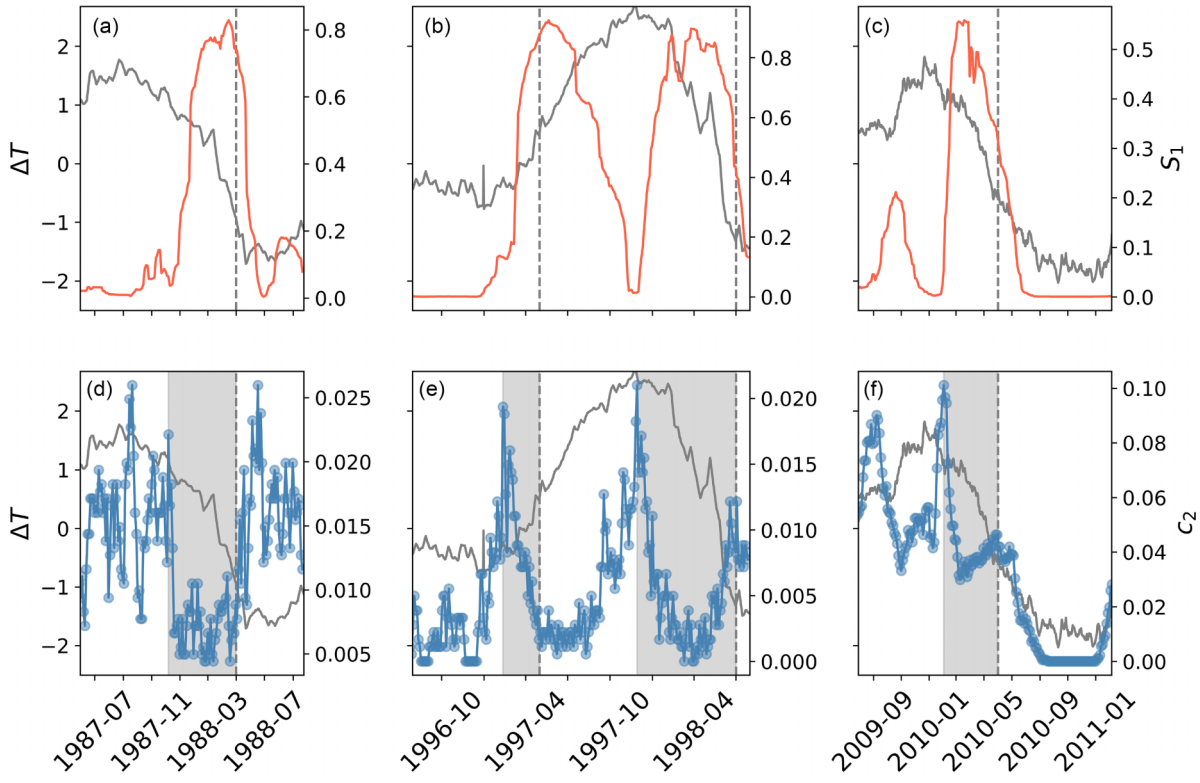

FIG. 6. (a–c) Average SST anomaly over the region 5S-5N/120W-170W, for three different periods (gray). The dashed vertical lines mark the beginning of El Niño/La Niña events. Relative size of the largest connected component S_1 (red) in the correlation network of SST built with correlation threshold $\gamma = 0.999$ for the first two periods and $\gamma = 0.998$ for the last period. (d–f) Probability c_2 that a randomly chosen node belongs to a component of size 2 in the correlation network of SST (blue). Reproducing of results from Rodriguez-Mendez *et al.* [40].

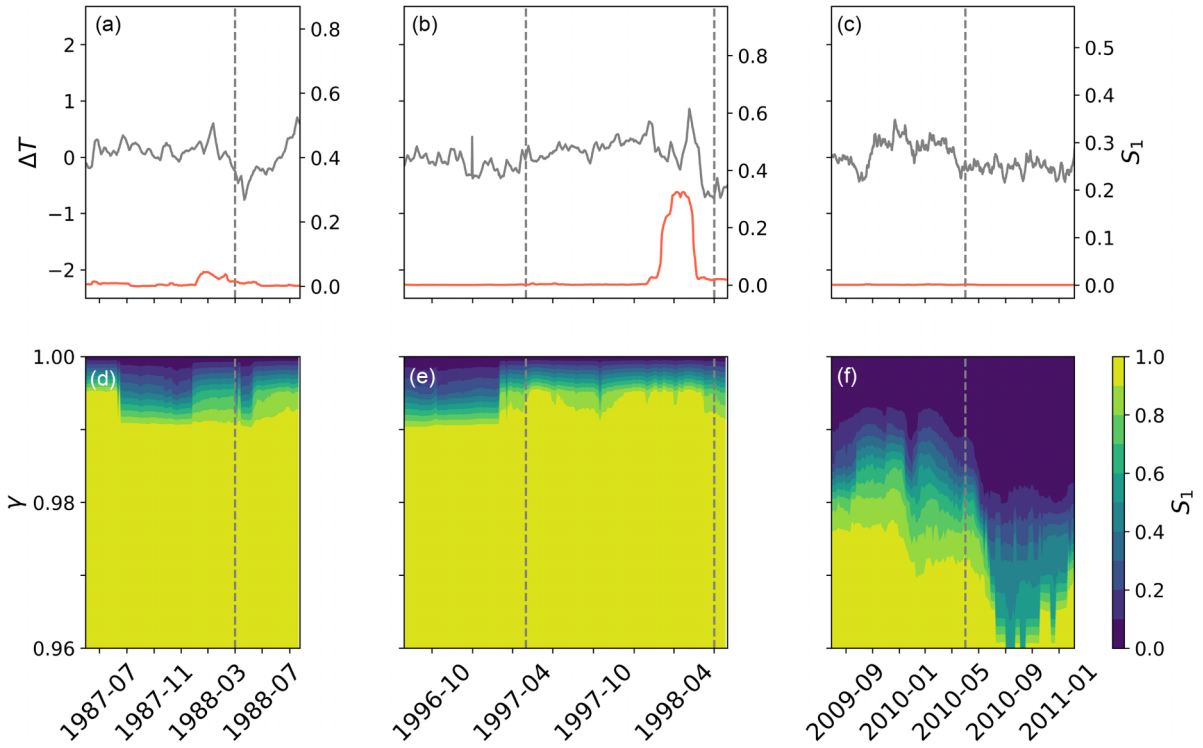

FIG. 7. (a–c) Average *detrended* SST anomaly over the region 5S-5N/120W-170W (gray). The dashed vertical lines mark the beginning of El Niño/La Niña events. Relative size of the largest connected component S_1 (red) in the correlation network of *detrended* SSTs built with correlation threshold $\gamma = 0.999$ for the first two periods and $\gamma = 0.998$ for the last period. (d–f) Values of S_1 for a range of correlation thresholds $\gamma \in [0.96, 1.00]$.

does not have an anticipatory value. A more detailed analysis would be required to identify its causes.

We can thus conclude that the increase in the size of the largest connected component preceding El Niño and La Niña events is due to a large-scale trend in the SSTs before every event, and not to a slowing down of the dynamics at some locations in space. This is relevant to discard possible mechanisms, as some models of ENSO obey a slow-fast structure very similar to the FN model [64]. The percolation precursors prove to be powerful tools to monitor the ENSO irregular oscillation, being sensitive enough to detect the emergent trend very early on and hence allowing for very early warning signals of approaching El Niño and La Niña events.

V. CONCLUSION

In summary, we have analyzed time-dependent functional networks encoding the evolution of correlations in spatially extended systems. The development of structures in such networks allows to detect subtle changes in the systems dynamics which might easily be overlooked by other analysis techniques. Precisely, we saw that the percolation precursors anticipate the abrupt changes between different stages of the oscillation in a system of coupled stochastic FitzHugh-Nagumo oscillators. The percolation reflects an increase in the correlations of the system which is due to the combination of two processes: (i) a global trend or coherent tendency among all spatial units preceding the abrupt change and (ii) an increase in the correlation of the noisy fluctuations "on top of" that trend (critical slowing down).

These considerations lead to a better understanding and interpretation of the percolation precursors in their application to the El Niño-Southern Oscillation. Our results demonstrate that the increase in correlation of sea surface temperatures over the NINO3.4 region preceding the studied El Niño and La Niña events is triggered by a large-scale trend in the SSTs, that is a growth or decay of the SSTs at all, or at least sufficiently many, spatial points, before every event and not by a slow down of the temperatures dynamics. This provides insights on the mechanism causing the performance of the percolation precursors in this particular case. We focused on a local scale, considering the El Niño basin only, and used instantaneous Pearson correlations in the network construction. Hence, our conclusions cannot be directly transferred to other percolation studies of El Niño which were performed on larger scales and used lagged-correlations such as in Refs. [43,46]. In those cases, the percolation is marked by the appearance of large-scale clusters and teleconnections, for which the causing factor remains to be found.

Tracking the structural changes in network descriptions of complex systems have the potential to reveal various dynamical aspects of these systems. Beyond the case of El Niño, these approaches have been utilized by Gupta *et al.* to track and identify short lived tropical cyclones [71]. Sun *et al.* [72] implemented a percolation model to investigate

the structure and complexity of the atmosphere. Fan *et al.* [73] have used a complex network framework to investigate changes in the atmospheric circulation associated with global warming and evaluate the impacts of future climate change. These examples suggest the potential of complex networks and their percolation properties to study present and future climate. Along this line, our work brings further insights into the situations in which the percolation-based precursors may be useful.

To facilitate future usage of the percolation framework described in this work, we provide in Ref. [74] a Python notebook performing the integration of the FitzHugh-Nagumo system with parameters specified in Sec. III and computing the correlation network as well as its percolation measures (Sec. II).

ACKNOWLEDGMENTS

This project has received funding from the European Union's Horizon 2020 research and innovation programme under the Marie Skolodowska-Curie Grant Agreement No. 813844, from the Agencia Estatal de Investigación (MCIN/AEI/10.13039/501100011033) under the María de Maeztu project CEX2021-001164-M, and from the Agencia Estatal de Investigación (MCIN/AEI/10.13039/501100011033) and FEDER "Una manera de hacer Europa" under Project LAMARCA No. PID2021-123352OB-C32. R.V.D. acknowledges financial support by the German Federal Ministry for Education and Research (BMBF) via the JPI Climate/JPI Oceans Project ROADMAP (Grant No. 01LP2002B).

[1] R. B. Alley, J. Marotzke, W. D. Nordhaus, J. T. Overpeck, D. M. Peteet, R. A. Pielke, R. T. Pierrehumbert, P. B. Rhines, T. F. Stocker, L. D. Talley, and J. M. Wallace, Science **299**, 2005 (2003).
[2] T. M. Lenton, H. Held, E. Kriegler, J. W. Hall, W. Lucht, S. Rahmstorf, and H. J. Schellnhuber, Proc. Natl. Acad. Sci. USA **105**, 1786 (2008).
[3] J. M. T. Thompson and J. Sieber, Int. J. Bifurcat. Chaos **21**, 399 (2011).
[4] P. Ashwin, S. Wieczorek, R. Vitolo, and P. Cox, Philos. Trans. R. Soc. A **370**, 1166 (2012).
[5] R. M. May, Nature (London) **269**, 471 (1977).
[6] M. Scheffer, S. Carpenter, J. A. Foley, C. Folke, and B. Walker, Nature (London) **413**, 591 (2001).
[7] W. Yan, R. Woodard, and D. Sornette, Phys. Procedia **3**, 1641 (2010).
[8] D. Smug, P. Ashwin, and D. Sornette, PLoS ONE **13**, e0195265 (2018).
[9] M. I. Maturana, C. Meisel, K. Dell, P. J. Karoly, W. D'Souza, D. B. Grayden, A. N. Burkitt, P. Jiruska, J. Kudlacek, J. Hlinka, M. J. Cook, L. Kuhlmann, and D. R. Freestone, Nat. Commun. **11**, 2172 (2020).
[10] M. Scheffer, J. Bascompte, W. A. Brock, V. Brovkin, S. R. Carpenter, V. Dakos, H. Held, E. H. van Nes, M. Rietkerk, and G. Sugihara, Nature (London) **461**, 53 (2009).
[11] M. Scheffer, S. R. Carpenter, V. Dakos, and E. H. van Nes, Annu. Rev. Ecol., Evol., Systemat. **46**, 145 (2015).
[12] T. M. Lenton, Nature Climate Change **1**, 201 (2011).
[13] C. Kuehn, J. Nonlinear Sci. **23**, 457 (2013).
[14] F. Romano and C. Kuehn, Int. J. Bifurcat. Chaos **28**, 1850103 (2018).
[15] F. Kwasniok, Chaos **28**, 033614 (2018).
[16] N. Boers, Nature Climate Change **11**, 680 (2021).
[17] C. Wissel, Oecologia **65**, 101 (1984).
[18] K. Wiesenfeld and B. McNamara, Phys. Rev. A **33**, 629 (1986).
[19] E. H. van Nes and M. Scheffer, Amer. Natural. **169**, 738 (2007).
[20] S. H. Strogatz, *Nonlinear Dynamics and Chaos: With Applications to Physics, Biology, Chemistry, and Engineering* (CRC Press, Boca Raton, FL, 2018).
[21] S. R. Carpenter and W. A. Brock, Ecol. Lett. **9**, 311 (2006).
[22] A. R. Ives, Ecol. Monogr. **65**, 217 (1995).
[23] H. Held and T. Kleinen, Geophys. Res. Lett. **31**, L23207 (2004).
[24] T. M. Lenton, V. N. Livina, V. Dakos, E. H. van Nes, and M. Scheffer, Philos. Trans. R. Soc. A **370**, 1185 (2012).
[25] V. Guttal and C. Jayaprakash, Ecol. Lett. **11**, 450 (2008).
[26] T. Kleinen, H. Held, and G. Petschel-Held, Ocean Dynam. **53**, 53 (2003).
[27] D. A. Seekell, S. R. Carpenter, and M. L. Pace, Amer. Natural. **178**, 442 (2011).
[28] F. Nazarimehr, S. Jafari, S. M. R. H. Golpayegani, and J. C. Sprott, Nonlin. Dynam. **88**, 1493 (2017).
[29] V. Guttal and C. Jayaprakash, Theoret. Ecol. **2**, 3 (2009).
[30] V. Dakos, S. Kéfi, M. Rietkerk, E. H. van Nes, and M. Scheffer, Amer. Natural. **177**, E153 (2011).
[31] S. R. Carpenter and W. A. Brock, Ecosphere **1**, 10 (2010).
[32] G. Tirabassi and C. Masoller, Chaos, Solitons Fractals **155**, 111720 (2022).
[33] G. Nicolis, A. G. Cantú, and C. Nicolis, Int. J. Bifurcat. Chaos **15**, 3467 (2005).
[34] M. Newman, *Networks* (Oxford University Press, 2010).
[35] H. A. Dijkstra, E. Hernández-García, C. Masoller, and M. Barreiro, *Networks in Climate* (Cambridge University Press, Cambridge, UK, 2019).
[36] J. Fan, J. Meng, J. Ludescher, X. Chen, Y. Ashkenazy, J. Kurths, S. Havlin, and H. J. Schellnhuber, Phys. Rep. **896**, 1 (2021).
[37] J. Ludescher, M. Martin, N. Boers, A. Bunde, C. Ciemer, J. Fan, S. Havlin, M. Kretschmer, J. Kurths, J. Runge, V. Stolbova, E. Surovyatkina, and H. J. Schellnhuber, Proc. Natl. Acad. Sci. USA **118**, e1922872118 (2021).
[38] M. van der Mheen, H. A. Dijkstra, A. Gozolchiani, M. Toom, Q. Feng, J. Kurths, and E. Hernandez–Garcia, Geophys. Res. Lett. **40**, 2714 (2013).
[39] G. Tirabassi, J. Viebahn, V. Dakos, H. Dijkstra, C. Masoller, M. Rietkerk, and S. Dekker, Ecological Complexity **19**, 148 (2014).
[40] V. Rodríguez-Méndez, V. M. Eguíluz, E. Hernández-García, and J. J. Ramasco, Sci. Rep. **6**, 29552 (2016).
[41] U. Feudel, A. N. Pisarchik, and K. Showalter, Chaos **28**, 033501 (2018).
[42] C. Kuehn, Physica D **240**, 1020 (2011).

[43] J. Meng, J. Fan, Y. Ashkenazy, and S. Havlin, Chaos **27**, 035807 (2017).
[44] Z. Lu, N. Yuan, and Z. Fu, Sci. Rep. **6**, 26779 (2016).
[45] Z. Lu, Z. Fu, L. Hua, N. Yuan, and L. Chen, Sci. Rep. **8**, 14912 (2018).
[46] R. Sonone and N. Gupte, Phys. Rev. E **103**, L040301 (2021).
[47] A. Radebach, R. V. Donner, J. Runge, J. F. Donges, and J. Kurths, Phys. Rev. E **88**, 052807 (2013).
[48] T. Kittel, C. Ciemer, N. Lotfi, T. Peron, F. Rodrigues, J. Kurths, and R. V. Donner, Eur. Phys. J.: Spec. Top. **230**, 3075 (2021).
[49] M. Wiedermann, A. Radebach, J. F. Donges, J. Kurths, and R. V. Donner, Geophys. Res. Lett. **43**, 7176 (2016).
[50] M. Gerster, R. Berner, J. Sawicki, A. Zakharova, A. Škoch, J. Hlinka, K. Lehnertz, and E. Schöll, Chaos **30**, 123130 (2020).
[51] Z. Neal and C. Rozenblat, *Handbook of Cities and Networks* (Edward Elgar Publishing, Cheltenham, UK, 2021).
[52] S. Abe and N. Suzuki, Physica A **337**, 357 (2004).
[53] J. F. Donges, Y. Zou, N. Marwan, and J. Kurths, Eur. Phys. J.: Spec. Top. **174**, 157 (2009).
[54] N. Ekhtiari, C. Ciemer, C. Kirsch, and R. V. Donner, Eur. Phys. J.: Spec. Top. **230**, 3019 (2021).
[55] P. Holme and J. Saramäki, Phys. Rep. **519**, 97 (2012).
[56] J. I. Deza, M. Barreiro, and C. Masoller, Chaos **25**, 033105 (2015).
[57] L. N. Ferreira, N. C. R. Ferreira, E. E. N. Macau, and R. V. Donner, Eur. Phys. J.: Spec. Top. **230**, 2973 (2021).
[58] D. Stauffer and A. Aharony, *Introduction To Percolation Theory* (Taylor & Francis, Oxford, UK, 2018).
[59] A. L. Hodgkin and A. F. Huxley, J. Physiol. **117**, 500 (1952).
[60] R. FitzHugh, Bull. Math. Biophys. **17**, 257 (1955).
[61] J. Nagumo, S. Arimoto, and S. Yoshizawa, Proc. IRE **50**, 2061 (1962).
[62] H. Bao, W. Liu, and M. Chen, Nonlin. Dynam. **96**, 1879 (2019).
[63] J. H. E. Cartwright, V. M. Eguíluz, E. Hernández-García, and O. Piro, Int. J. Bifurcat. Chaos **09**, 2197 (1999).
[64] F.-F. Jin, J. Atmos. Sci. **54**, 811 (1997).
[65] R. Toral and P. Colet, *Stochastic Numerical Methods: An Introduction for Students and Scientists* (Wiley-VCH Verlag GmbH & Co. KGaA, Weinheim, Germany, 2014).
[66] E. Meron, Phys. Rep. **218**, 1 (1992).
[67] H. A. Dijkstra, *Nonlinear Climate Dynamics* (Cambridge University Press, Cambridge, UK, 2013).
[68] P. D. Nooteboom, Q. Y. Feng, C. López, E. Hernández-García, and H. A. Dijkstra, Earth Syst. Dynam. **9**, 969 (2018).
[69] H. A. Dijkstra, P. Petersik, E. Hernández-García, and C. López, Front. Phys. **7**, 153 (2019).
[70] D. P. Dee, S. M. Uppala, A. J. Simmons, P. Berrisford, P. Poli, S. Kobayashi, U. Andrae, M. A. Balmaseda, G. Balsamo, P. Bauer, P. Bechtold, A. C. M. Beljaars, L. van de Berg, J. Bidlot, N. Bormann, C. Delsol, R. Dragani, M. Fuentes, A. J. Geer, L. Haimberger *et al.*, Quart. J. Roy. Meteorol. Soc. **137**, 553 (2011).
[71] S. Gupta, N. Boers, F. Pappenberger, and J. Kurths, Clim. Dynam. **57**, 3355 (2021).
[72] Y. Sun, J. Meng, Q. Yao, A. A. Saberi, X. Chen, J. Fan, and J. Kurths, Phys. Rev. E **104**, 064139 (2021).
[73] J. Fan, J. Meng, Y. Ashkenazy, S. Havlin, and H. J. Schellnhuber, Proc. Natl. Acad. Sci. USA **115**, E12128 (2018).
[74] N. Ehstand, https://github.com/noemiee/FitzHugh-Nagumo-percolation-analysis.git (2023).